# Photoluminescence of Ag+ and Ag m n+ in co-doped Pr3+/Yb3+ fluorophosphate glasses: tuning visible emission and energy transfer to Pr3+/Yb3+ ions through excitation in different silver species

Tarcio Castro, Veronique Jubera, Hssen Fares, Yannick Petit, Alexandre Fargues, Thierry Cardinal, Marcelo Nalin, Sidney Ribeiro

# Photoluminescence of $Ag^{+}$ and $Ag_m^{n+}$ in co-doped $Pr^{3+}/Yb^{3+}$ fluorophosphate glasses: tuning visible emission and energy transfer to $Pr^{3+}/Yb^{3+}$ ions through excitation in different silver species

Tarcio Castro[a,b], Véronique Jubera[b], Hssen Fares[a,b], Yannick Petit[b,c], Alexandre Fargues[b], Thierry Cardinal[b], Marcelo Nalin[a] and Sidney Ribeiro[a].

[a]*Institute of Chemistry - São Paulo State University - UNESP, CP 355, Araraquara, SP, 14800-060, Brazil.*

[b]*University of Bordeaux, CNRS, ICMCB, UPR 9048, 87 avenue du Dr. A. Schweitzer, 33608 Pessac cedex, France*.

[c]*University of Bordeaux, CNRS, CEA, CELIA, UMR 5107, 351 Cours de la Liberation, 33405 Talene Cedex, France.*

**Keywords:** fluorophosphate glasses, rare earths, Ag nanoclusters and energy transfer.

## Abstract

Here, we report the luminescence properties of $Yb^{3+}/Pr^{3+}$ dual-doped fluorophosphate glasses containing silver clusters. Through the solubility of silver into the glass system as function of its initial concentration, charged species characterized as $Ag^{+}$ and $Ag_m^{n+}$ were formed and identified according to their absorption and emission spectral responses. By changing the transition metal concentration, multi-energy transfer mechanisms were observed between silver and $Yb^{3+}/Pr^{3+}$ co-doped glasses. The stabilization of silver species seems to be detrimental to the radiative processes of the rare earth ions under excitation at 444 nm ($Pr^{3+}$ $^3H_4 \rightarrow {}^3P_0$ absorption line). In other words, the main visible emissions of $Pr^{3+}$ and the NIR emission of $Yb^{3+}$ decrease with increment of Ag concentration. However, energy transfer occurs for large spectral range by the excitation of the silver species. In consequence, the visible and NIR emission could be activate in a broadband from ultraviolet to the blue part of the spectral region. These two observations highlight the competitive absorption processes

and probabilities between the cationic elements and the interest to use the transition metal species as sensitizers to excite the rare earth elements.

**Introduction**

Materials containing metal ions, such as silver have paved new advances in modern spectroscopy. Counting with the rich optical properties of silver nanoclusters and nanoparticles, new materials have been developed for numerous applications like solar cell efficiency enhancement [1], light frequency converter [2], white light generation [3,4] and others [5-7]. The large UV-Vis absorption and emission is ascribed to the evolution of certain charged and uncharged silver species like, for example, $Ag^{+}$, $Ag^{0}$, and $Ag_m^{n+}$ [8,9]. $Ag_m^{n+}$ centers result from aggregation of y silver ions $Ag^{+}$ and z silver atoms $Ag^{0}$ forming $Ag_m^{n+}$ charged nanoclusters (m=y+z and n=y) [10]. Moreover, taking into account the energy levels and the size of the $Ag_m^{n+}$ species, broad absorption and emission spectra can be observed [11,12], making such clusters suitable for efficiently transfer energy to rare earth (RE) ions [13,14]. In one of the first publication regarding NC's-RE interaction, Tikhomirov *et al*., reported an energy transfer (ET) between $Ag_m^{n+}$ and $Yb^{3+}$ in oxyfluoride glasses [15]. In that case, the $Yb^{3+}$ ions emission at 1000 nm was achieved by resonant and non-resonant excitation in $Ag_m^{n+}$. Huiyun Wang *et al*., studied a broadening excitation by co-doping oxyfluoride glass resulting in a energy transfer Ag clusters → $Yb^{3+}$ ions and simultaneous energy transfer Ag clusters → $Eu^{3+}$ → $Yb^{3+}$. Recently, Zhuang Guo *et al*., proved that $Ag_m^{n+}$ is an efficient broadband sensitizer for $Sm^{3+}$ ions in the visible range [16] via energy transfer Ag clusters → $Sm^{3+}$. From these studies we conclude that $RE^{3+}$ energy levels may be assessed via Ag clusters energy transfer.

Size-dependent of the $Ag_m^{n+}$ species have been investigated in different glass hosts. Previous publications indicate that many factors might affect the size distribution of Ag species, such as heat treatment, Ag concentration, glass network changes and RE doping [17-20]. Concomitantly, in a system that presents rare earth ions, $Ag_m^{n+}$ may benefit ET interactions in such a way that visible and near-infrared emissions of $RE^{3+}$ ions may be sensitized and enhanced [21,22]. Indeed, the forbidden character of 4*f* - 4*f* transition make the UV-Vis

cross-section of the $RE^{3+}$ small. On the other hand, the presence of Ag entities can boost the absorption efficiency, in this sense an efficient interaction among RE and $Ag_m^{n+}$ can globally enhance the luminescence [23].

In this work, fluorophosphate glasses with molar composition $30NaPO_3$-$30MgF_2$-$30BaF_2$-$10YF_3$ were prepared via melt-quenching method by co-doping with $Pr^{3+}$/$Yb^{3+}$ and different silver contents. We investigate the luminescence properties of the $Pr^{3+}$/$Yb^{3+}$ ions as a function of the silver concentration. In addition, the broadband excitation and emission of the Ag species were studied as well as their interaction with rare earth ions.

## 2. Experimental section

### 2.1 Glass preparation

The glass samples were prepared by the melt-quenching method with the following chemical batch composition (mol %): (29-x) $NaPO_3$–$30MgF_2$–$30BaF_2$–$10YF_3$–$0.5Pr_2O_3$-$0.5YbF_3$ – $xAgNO_3$ (x = 0, 2 and 10) with, approximately, 5 g to each. All compounds used were 99.9 % purity (Sigma Aldrich). The raw materials were thoroughly mixed in a speed mixer with 1000 rpm, transferred to an alumina crucible and melted at 800 °C for 30 min in ambient atmosphere to eliminate nitrates and have a homogeneous liquid. The melt was poured onto a stainless-steel mold, preheated at 340 °C and kept at this temperature for 2 h to reduce mechanical stress due to the fast cooling. Table 1 summarizes the sample compositions: the amount of $Pr_2O_3$ and $YbF_3$ raw materials introduced were fixed at 0.5 mol% and $AgNO_3$ concentration between 0 and 10 mol % resulting from the $AgNO_3$ introduced in the batch. To verify the effect of silver ions in the emission and excitation spectrum, a sample without silver was prepared. Still, for comparison, a sample without $Pr^{3+}$ ions was also prepared to evidence the energy transfer from the silver species present in the glass network ($Ag_m^{n+}$ and $Ag^+$) to the $Yb^{3+}$ ions.

Table 1. Molar compositions of the raw materials and samples label.

| Compounds (mol%) | | | | | | | |
|---|---|---|---|---|---|---|---|
| $NaPO_3$ | $MgF_2$ | $BaF_2$ | $YF_3$ | $Pr_2O_3$ | $YbF_3$ | $AgNO_3$ | Label |
| 30 | 30 | 30 | 10 | 0 | 0 | 0 | **Pure host** |
| 29 | 30 | 30 | 10 | 0.5 | 0.5 | 0 | **PYAg0** |
| 27 | 30 | 30 | 10 | 0.5 | 0.5 | 2 | **PYAg2** |
| 19 | 30 | 30 | 10 | 0.5 | 0.5 | 10 | **PYAg10** |
| 19.5 | 30 | 30 | 10 | 0 | 0.5 | 10 | **YAg10** |

## 2.2 Characterizations

Absorption spectra were recorded using a Carry 5000 Spectrometer (Varian) double-beam coupled with resolution of 1 nm. The excitation and emission spectra were collected in a Horiba Jobin Yvon Fluorolog 3 equipped with Xenon lamp (450 W), an InGaAs detector and a photomultiplier tube (PMT - Hamamatsu R298) for the infrared detection and visible signal, respectively. All measurements were performed at room temperature and the samples were grinded in order to avoid re-absorption process. Emission spectra were corrected from the lamp intensity variation, configuration geometry and detectors sensitivity.

## 3. Results and discussions

### 3.1 Absorption Spectra

The absorption spectra of the prepared samples are depicted in Figure 1. The non-doped matrix absorption spectrum (black line) is illustrated to discriminate the rare earth and silver absorption. The PYAg0 curve clearly evidenced the insertion of $Pr^{3+}$ and $Yb^{3+}$ ions in the glass. $Pr^{3+}$ doped glass shows four groups of lines ranging from 400 to 650 nm attributed to *4f-4f* absorption lines, which are emphasized on the inset graph. These peaks correspond to the $^3H_4 \rightarrow {}^3P_2$, $^3P_1$, $^3P_0$ and $^1D_2$ excited states transitions and are located at 445, 469, 482 and 580-610 nm respectively. The $Yb^{3+}$ ($^2F_{7/2} \rightarrow {}^2F_{5/2}$) absorption lines are visible at around 980 nm. As compared to the reference (pure host), no real influence of the rare earth doping is evidenced at high energy as the charge transfer band (CTB)

between $Yb^{3+}$ and the ligands or the *4f-5d* absorption band of $Pr^{3+}$ are both expected at smaller wavelength than the absorption threshold observed. The cut-off from the pure host (black line) starts in 300 nm, and this limit is shifted to longer wavelengths when the concentration of silver amounts increases. For the highest silver concentration, the absorption due to silver species clearly overlaps the absorption lines of the $Pr^{3+}$ ions. Their contribution appears as shoulder on the curves. In addition, a higher silver concentration reduces the transparency in the visible due to the brown color of the samples (see inset digital pictures in Figure 1). This color is attributed to the increases of particle size as a function of Ag amount (Ag NC's aggregate and tend to adopt a metallic behavior) and/or to the formation of Ag NP's [25].

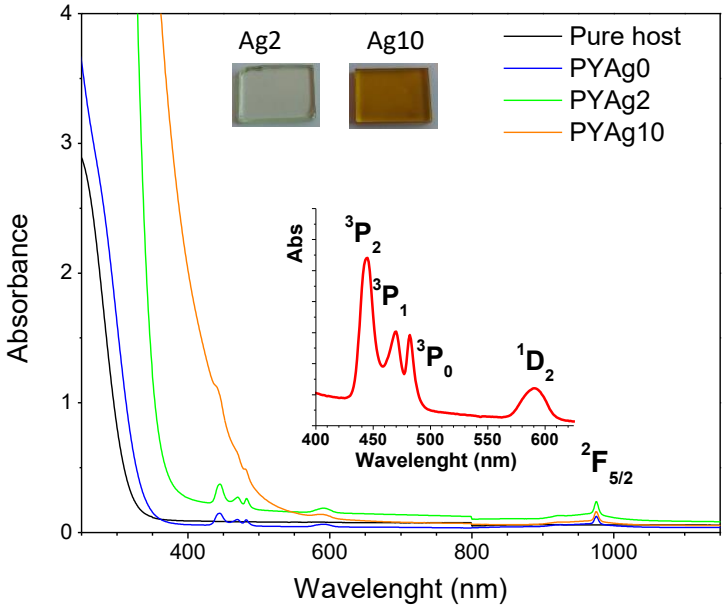


Figure 1. Absorption spectra of the pure host (black line), co-doped with $Pr^{3+}/Yb^{3+}$ and different silver amount. The inset shows $Pr^{3+}$ absorption lines in the visible range for the sample PYAg0 (without silver oxide introduced) and the digital pictures show the change in color as a function of the Ag content.

### 3.2 Spectroscopic Results

In order to evaluate the spectroscopic properties of $Ag^{+}$ and $Ag_m^{n+}$ species and their interaction with the rare earth ions, we dedicated a deeper attention to the photoluminescent properties.

First, the emission spectra collected for excitation at 444 nm wavelength associated to $Pr^{3+}$ ions $^3H_4 \rightarrow {}^3P_2$ transition are illustrated for the different samples in Figure 2.

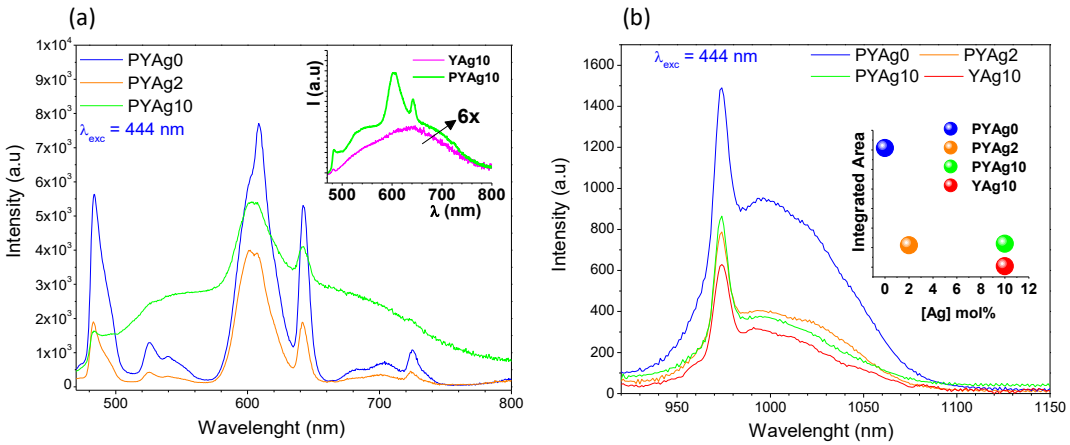


Figure 2. Emission curves of $PYAg_x$ glasses (x= 0, 2, 10) under excitation at 444 nm in the $^3P_2$ level of $Pr^{3+}$ ions. a) The acquisition in the visible range shows the contribution of silver species in addition to $Pr^{3+}$ lines; b) Luminescence of $Yb^{3+}$ ions is clearly detected in the infrared range at around 1000 nm.

Under such an excitation ($Pr^{3+}$: $^3H_4 \rightarrow {}^3P_2$), the radiative de-excitation from $^3P_0$ $Pr^{3+}$ level is clearly detected in the visible range (Figure 2a). The main emissions are centered at around 486 nm, 580-620 nm and 700 nm, which correspond to the radiative transitions $^3P_0 \rightarrow {}^3H_4$, $^1D_2 \rightarrow {}^3H_4$, $^3P_0 \rightarrow {}^3H_6$ and $^3P_0 \rightarrow {}^3F_2$, respectively. The nature of the emitting levels of $Pr^{3+}$ strongly depends on the phonons energy of the host. Radiative de-excitation from $^1D_2$ level were reported in fluorophosphates [25], fluoroindate glasses [26], lead borate [27] glasses, as well as, oxyfluoride silicate glass–ceramics [28], whereas this level relaxes non radiatively down to the $^1G_4$ level in ZBLAN glass [29]. With the addition of silver ions, the $Pr^{3+}$ emissions decrease in intensity and a broadband rises, covering the region between 480 and 800 nm. The quenching of the green emission ($^3P_0 \rightarrow {}^3H_4$) is more accentuated compared to the red one (overlap between $^1D_2 \rightarrow {}^3H_4$ and $^3P_0 \rightarrow {}^3H_6$ lines). For the silver containing sample with x=10, the 486 nm green line almost disappeared. The persistence of a red component seems to confirm that, in the proposed materials, the potential de-

excitation from $^1D_2$ to $^1G_4$ level, if existing, is limited. For comparison, the inset of the Figure 2a shows the emission of the sample for x=10 without $Pr^{3+}$ ions (pink line) under the same excitation (444 nm); in this case, we can see a wide emission that is similar to the rare earth co-doped sample containing silver (x=10).

Second, the excitation at 444 nm makes also possible the observation of the $Yb^{3+}$ $^2F_{5/2} \rightarrow {}^2F_{7/2}$ transition, pointing out energy transfer from $Pr^{3+}$ ions to the $Yb^{3+}$ ions. Several mechanisms can be proposed to illustrate such energy transfer. (1) A cross-relaxation between the $^3P_0 \rightarrow {}^1G_4$ $Pr^{3+}$ transition and the $^2F_{7/2} \rightarrow {}^2F_{5/2}$ transition of $Yb^{3+}$ ions. This is followed by a multiphonon relaxation from $^1G_4$ down to lower energy levels and a radiative de-excitation of one $Yb^{3+}$ excited from the $^2F_{5/2}$ level. (2) Another potential mechanism could be a resonant two-step energy transfer: the cross-relaxation process proposed before could be followed by a second transfer step involving the $^1G_4 \rightarrow {}^3H_4$ $Pr^{3+}$ line and $^2F_{7/2} \rightarrow {}^2F_{5/2}$ absorption. This second scheme should make possible the emission of two photons at around 1 micron. (3) A third cross relaxation process could occur between the $^1D_2 \rightarrow {}^3F_4$ transition of $Pr^{3+}$ and $^2F_{7/2} \rightarrow {}^2F_{5/2}$ transition of $Yb^{3+}$ ions. In this case, the excited $Yb^{3+}$ ion relaxes radiatively by emitting one photon and the $^3F_4 \rightarrow Pr^{3+}$ level implies multiphonon de-excitation mechanism. (4) Depending on the system and concentration, back energy transfer from $Yb^{3+}$ to $^1G_4$ level of $Pr^{3+}$ can be observed [26,29,30]. These mechanisms may be easily accessed in the Figure 6.

Under a 444 nm excitation, the intensity of the infrared emission is strongly affected by the introduction of silver in the glass composition (the integrated intensity as function of silver content is reported in the inset of Figure 2b). However, energy transfer from praseodymium ions seems to compete with a potential back transfer from $Yb^{3+}$ ions to other ions: the intensity of PYAg10 is superior to that of YAg10 sample (Figure 2b).

Excitation spectra performed for the most intense lines of $Pr^{3+}$ ($\lambda_{em}$ = 606 nm) and $Yb^{3+}$ ($\lambda_{em}$ = 980 nm) ions are illustrated in Figure 3a and 3b respectively. In addition to the $Pr^{3+}$ absorption lines (lines peaking at 445, 469, 482 and 580-610 nm, see also Figure 1), the broadband ranging between 250 to 500 nm (Figure 3a), is attributed to silver species. This overlapping of silver and

praseodymium excitation bands is a clear evidence of energy transfer between the $Pr^{3+}$ ions and silver species. Broad excitation bands between 250 to 500 nm (Figure 3b) are also detected in the excitation spectrum of $Yb^{3+}$ ions, showing the energy transfer pathway to this rare earth element.

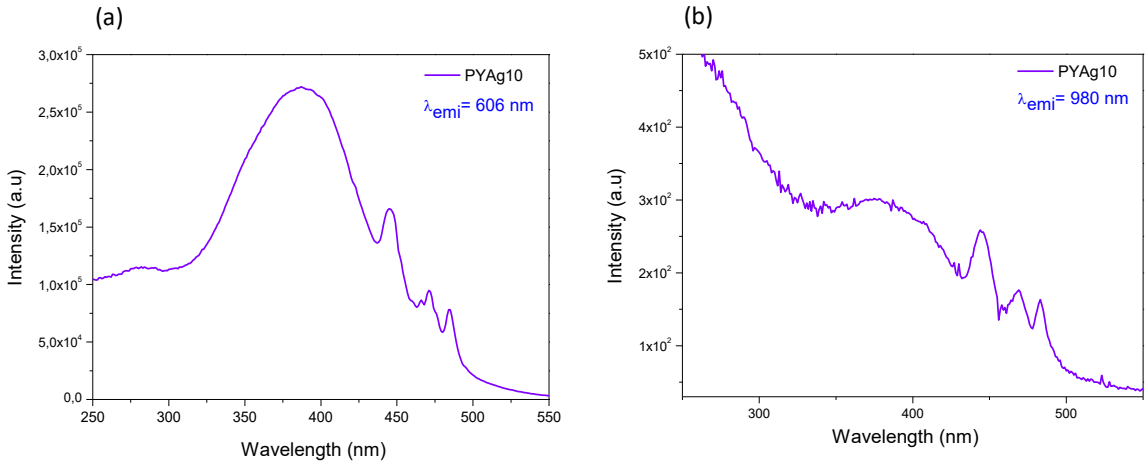


Figure 3. Excitation spectra of the sample PYAg10 with emission fixed at 606 and 980 nm.

To discriminate the contribution of rare earth elements from that of silver species, excitation spectra were collected for a fixed emission wavelength at 564 nm for which no emission from $Pr^{3+}$ ions is observed. The corresponding spectra obtained for different silver content are illustrated in the Figure 4.

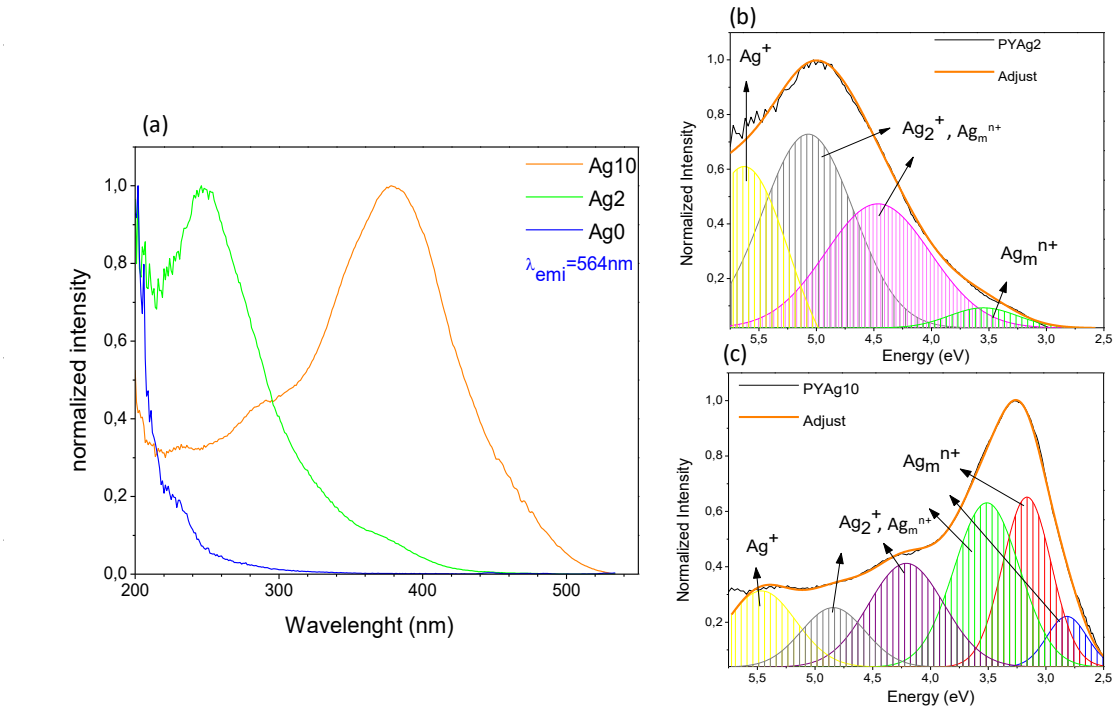


Figure 4. Excitation spectra of $PYAg_x$ glasses (x= 0, 2, 10) for an emission wavelength fixed at 564 nm (a). Deconvolutions of the excitation bands for the samples PYAg2 (b) and PYAg10 (c).

The excitation curves revealed different bands. The relative intensity of these bands is modulated with the silver concentration meaning that the $PYAg_x$ glasses stabilize several species of silver depending on the silver concentration introduced and are assigned to various silver species. The spectral signature depends on the ion distribution, as well as the local environment around the silver species [26]. The deconvolution spectra point an absorption band at 230 nm (5.5 eV) that can be attributed to $Ag^+$ ions [31]. The bands ranging from 250 nm to 310 nm (≈5.2eV - 4eV) overlap the absorption of silver pairs $(Ag^+)_2$ and $Ag_m^{n+}$ silver clusters whereas the band peaking at the lowest energy could be compatible to the stabilization of $Ag_m^{n+}$ clusters [31-33]. The noticeable number of silver species indicates a low dispersion of Ag in this glass system with silver aggregation starting for x = 2. In this concentration, two main excitation bands are observed around 250 nm and 280 nm, whose are assigned to the $^3D_1 \rightarrow {}^1S_0$ $Ag^+$ transition [27]. Still, for 2 mol% the formation of $Ag_m^{n+}$ start to be relevant. One can notice a weak excitation band at around 370 nm which is attributed to

$Ag_m^{n+}$ species. In relative intensity the excitation band attributed to $Ag^+$ is not dominant for x=10.

Figure 5 shows the emission spectra of the samples with different excitation wavelengths in agreement with the deconvolution proposed in Figure 4: 240 nm, 370 nm and 420 nm excitation wavelengths. Visible emissions are shown on the up side (5a, 5c and 5e) and the near-infrared on the bottom (5b, 5d and 5f). In the visible range, the main emission is due to contribution of the silver species ($Ag^+$ and $Ag_m^{n+}$). The excitation at 240 nm results in a large band located at around 400 nm. For such an excitation, a decrease of the emission intensity is observed with the increase of silver content. The 370 nm and 420 nm excitations give rise to two bands peaking at 500 nm and 650 nm, respectively. The intensity of these two contributions clearly increases with the silver content in a good coherence with the evolution of the silver species nature stabilized in the glasses. In addition, a weak contribution of $Pr^{3+}$ ions is also visible and the $Yb^{3+}$ $^2F_{5/2} \rightarrow {}^2F_{7/2}$ transitions are detected in the infrared. In our case, if we cannot totally discard the existence of silver metallic nanoparticles, an effect of the surface plasmon resonance is not expected. Still, our investigation also tends to emphasize that the $Pr^{3+}$ and $Yb^{3+}$ emission is observed by direct excitation of silver species, although a small emission is observed at around 600 nm, which corresponds to the $Pr^{3+}$ transition ($^1D_2 \rightarrow {}^3H_4$). Thus, emissions from silver species become an interesting channel to excite the rare earth cations. For the sake of brevity, we present here only results from three excitation wavelengths (240 nm, 370 nm and 420 nm). However, the rare earth ions luminescence can be detected when the excitation is carried out in a wide range of the $Ag^+$ and $Ag_m^{n+}$ response (270 nm to 420 nm). The $Yb^{3+}$ ions emission is also visible in the $Pr^{3+}$ free sample (red line in Figures 5b, 5d and 5f). This $Ag^+$, $Ag_m^{n+} \rightarrow Yb^{3+}$ energy transfer was also reported for oxyfluoride system [33]. For the $Yb^{3+}$ emission the 5 → 1 zero phonon line is clearly visible whereas the other components related to the radiative de-excitation from the lowest Stark component of the $^2F_{5/2}$ level down to the fundamental multiplet (Transitions 5 → 2, 3, 4) are merged into a large band as observed previously for the excitation at 444 nm in the $Pr^{3+}$ ions absorption.

The inset graphics from the Figure 5 show the integrated intensities of the visible and NIR emission. As discussed previously, the $Ag^+$ ions being the

dominant specie (sample PYAg2), an excitation at 240 nm leads to a more efficient energy transfer to the $Pr^{3+}$ and $Yb^{3+}$ cations for the lowest silver content glasses: $Ag^{+}$ and rare earth ions emissions decrease with the increase of silver content in the glass (Figures 5a and 5b). This observation is consistent with the decrease in concentration of isolated silver ions $Ag^{+}$ in the glass for high silver loading. However, the rare earth cations emission increases with the silver content for excitations above 300 nm corresponding to the excitation wavelength range of the $Ag_m^{n+}$ species (Figures 5c, 5d, 5e and 5f).

For an excitation at 444 nm corresponds to both an absorption of the $Pr^{3+}$ lines and the $Ag_m^{n+}$ species (Figure 3b). The competitive absorption affects the emission intensity of the rare earth and the transfer from $Pr^{3+}$ ions to $Yb^{3+}$ ions.

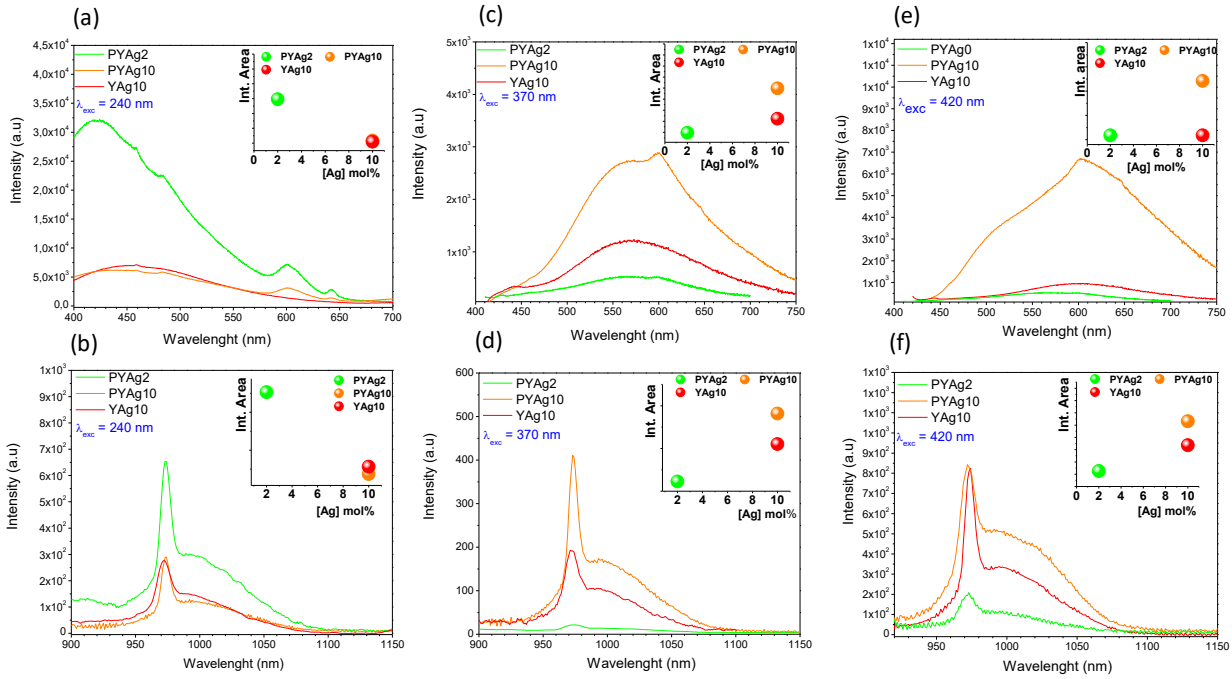


Figure 5. Emission spectra in the visible range (a, c and e) and near-infrared (b, d and f) performed under excitation in silver species. The broadband visible emissions characterizes the Ag and $Ag_m^{n+}$ species and an ET is observed by the weak emission of $Pr^{3+}$ at around 600 nm.

Finally, different energy mechanisms can be proposed as function of the silver species nature. Figure 6 shows the partial diagram of energy levels of the

$Pr^{3+}/Yb^{3+}$ co-doped samples and containing $Ag^{+}$ and $Ag_m^{n+}$ species accordingly with the energy diagram proposed by Velazquez et al. [34].

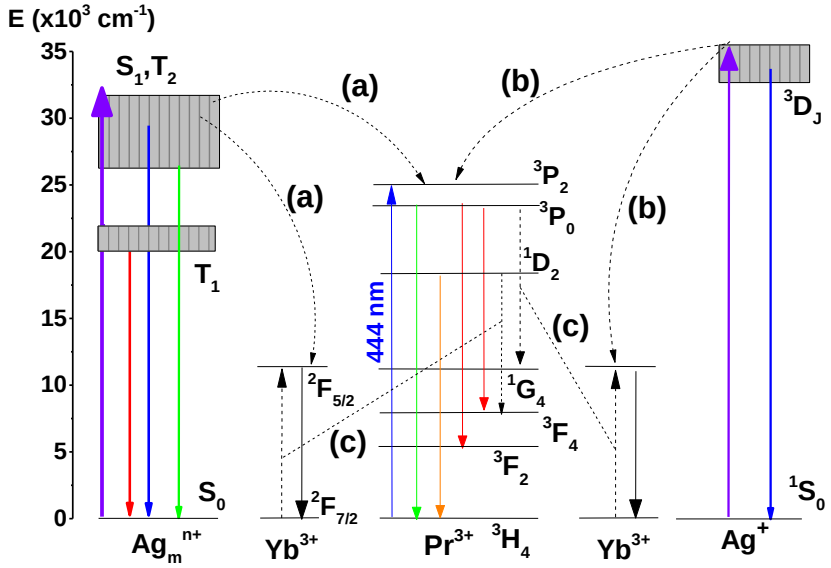


Figure 6. Partial diagram of energy levels of co-doped $Pr^{3+}/Yb^{3+}$, $Ag^{+}$ and $Ag_m^{n+}$ in fluorophosphate glass; **a** and **b** denote energy transfer and **c**, cross relaxation.

The blue, green and red emission rise respectively from the radiative transitions of the excited states $S_1$, $T_2$ and $T_1$ to the ground state $S_0$ in the $Ag_m^{n+}$ clusters [14,35]. The energy states of the silver nanoclusters vary significantly due to the non-shielded 3d orbitals. Thus, the $Ag_m^{n+}$ may be excited in a broad range of the UV light and part of the visible radiation, from 240 nm up to 444 nm. In contrast, the 4f energy levels of the $Pr^{3+}$ and $Yb^{3+}$ result from weak interactions with the closest neighbor in the glass network. Upon 444 nm excitation, the $Pr^{3+}$ ions excite electrons from the ground state $^3H_4$ to the excited states $^3P_2$, $^3P_1$, $^1I_6$, $^3P_0$ and $^1D_2$. The excited state of the $Yb^{3+}$ can be activated by energy transfer from the $Ag^{+}$ and $Ag_m^{n+}$ species or by cross relaxation between the $Pr^{3+}$ and $Yb^{3+}$ ions.

## 4. Conclusions

In summary, silver containing fluorophosphate glasses co-doped with $Pr^{3+}/Yb^{3+}$ were prepared by the melting quenching method. Different silver species from silver ions to silver clusters were obtained depending on the silver amount introduced. Energy transfers have been evidenced between the silver species and the rare earth ions. Thanks to the absorption of the silver species, a broad band in the visible range become accessible for the excitation $Pr^{3+}$ and $Yb^{3+}$ rare earth ions. At short wavelength excitation (240 nm) the $Ag^{+}$ ions response predominates under the visible and NIR emission from the $Pr^{3+}$ and $Yb^{3+}$ ions, respectively. At this excitation the increment of the Ag concentration leads to a quenching of the rare earths luminescence. However, for longer wavelength (> 370 nm) the rare earths ions emissions become more evident and increase with the Ag increment. This approach point out hopeful perspectives to explore a new approach for down-conversion layers and phosphors.

## Acknowledgments

The authors are grateful for the financial support from the Brazilian agencies CAPES, CNPq, grants numbers #2018/09296-3, #2016/16343-2 and #2013/07793-6, São Paulo Research Foundation – FAPESP and the French agencies CNRS, the Cluster of Excellence LAPHIA (ANR-10-IDEX-03-02) and the Region “Nouvelle Aquitaine” in the frame of the FabMat project (2016-1R10107).

## References

1. F. Enrichi, C. Armellini, G. Battaglin, F. Belluomo, S. Belmokhtar, A. Bouajaj, E. Cattaruzza, M. Ferrari, F. Gonella, A. Lukowiak, M. Mardegan, S. Polizzi, E. Pontoglio, G.C. Righini, C. Sada, E. Trave, L. Zur, Opt. Mater. **60**, 249–269 (2016).

2. Ronghua Ma, Jiangyun Qian, Shuo Cui, Xvsheng Qiao, Feng Wang, Xianping Fan, J. Lumin. **152**, 222–225 (2014).

3. Ronghua Ma, Jun Gao, Xu Qian, Shuo Cui, Xvsheng Qiao, Du Jincheng, Xianping Fan, J. Non-Cryst. Solids **432**, 348–353, (2016).

4. J.J. Li, J.D. Chen, R.F. Wei, H. Guo, J. Am. Ceram. Soc. **95**, 1208–1211, (2012).

5. J.-C. Desmoulin, Y. Petit, L. Canioni, M. Dussauze, M. Lahaye, H.M. Gonzalez, E. Brasselet, T. Cardinal, J. Appl. Phys. **118**, 213104 (2015).

6. A. Khalil, J.-P. Bérubé, S. Danto, J.-C. Desmoulin, T. Cardinal, Y. Petit, R. Vallée, L. Canioni, Sci Rep **7**, 1–9, (2017).

7. A.S. Kuznetsov, V.K. Tikhomirov, M.V. Shestakov, V.V. Moshchalkov, Nanoscale **5**, 10065–10075, (2013).

8. Song Ye, Zhuang Guo, Huiyun Wang, Song Li, Tianhua Liu, Deping Wang, J. Alloy. Compd. **685**, 891–895, (2016).

9. Sungmoon Choi, Robert M. Dickson, Yu. Junhua, Chem. Soc. Rev. **41**, 1867–1891, (2012).

10. I. Diez, R.H.A. Ras, Nanoscale **3**, 1963–1970, (2011).

11. W.P. Halperin, Rev. Mod. Phys. **58**, 533–606, (1986).

12. Zhuang Guo, Song Ye, Xvsheng Qiao, Deping Wang, J. Am. Ceram. Soc. **00**, 1–7, (2017).

13. D. Rajesh, R.J. Amjad, M. Reza Dousti, A.S.S. de Camargo, Journal of Alloys Compounds. **695**, 607–612, (2017).

14. José A. Jiménez, J. Inorg. Organomet. Polym Mater. **27**, 372–379, (2017).

15. V.K. Tikhomirov, V.D. Rodríguez, A. Kuznetsov, D. Kirilenko, G. Van Tendeloo, V.V. Moshchalkov, Opt. Express **21**, 22032–22040, (2010).

16. Zhuang Guo, Song Ye, Tianhua Liu, Song Li, Deping Wang, J. Non-Cryst. Solids **458**, 80–85, (2017).

17. V.D. Dubrovin, Opt. Mater. **36**, 753–759 (2014)

18. A.S. Kuznetsov, N.T. Cuong, V.K. Tikhomirov, M. Jivanescu, A. Stesmans, L.F. Chibotaru, J.J. Velázquez, V.D. Rodríguez, D. Kirilenko, G. Van Tendeloo, V.V. Moshchalkov, Opt. Mater. **34**, 616–621, (2012).

19. Ronghua Ma, Junjie Zhao, Xiaotong Chen, Xvsheng Qiao, Xianping Fan, Du Jincheng, Xianghua Zhang, Phys. Chem. Chem. Phys. **19**, 22638–22645, (2017).

20. Qing Jiao, Jianbei Qiu, Dacheng Zhou, Xu Xuhui, Mater. Res. Bull. **51**, 315–319, (2014).

21. Longji Li, Yong Yang, Dacheng Zhou, Zhengwen Yang, Xu Xuhui, Jianbei Qiu, Opt. Mater. Express **6**, 806–812, (2013).

22. Wu Yi, Xiang Shen, Shixun Dai, Xu Yinsheng, Feifei Chen, Changgui Lin, Xu Tiefeng, Qiuhua Nie et al., J. Phys. Chem. C **115**, 25040–25045, (2011).

23. RongFei Wei, JingJing Li, JiaYu. Gao, Hai Guo, J. Am. Ceram. Soc. **95**, 3380–3382, (2012).

24. M.C. Mathpal, P. Kumar, S. Kumar, A.K. Tripathi, M.K. Singh, J. Prakash, A. Agarwal, RSC Adv. **5**, 12555–12562, (2015).

25. S. Babu, P. Rajput, Y.C. Ratnakaram, J. Mater. Sci. **51**, 8037–8054, (2016).

26. L.J. Borrero-González, G. Galleani, D. Manzani, L.A.O. Nunes, S.J.L. Ribeiro, Opt. Mater. **35**, 2085–2089, (2013).

27. D. Serrano, A. Braud, J.L. Doualan, P. Camy, A. Benayad, V. Ménard, R. Moncorgé, Opt. Mater. **33**, 1602–1606, (2011).

28. Gu Mu, Qing-Chun Gao, Shi-Ming Huang, Xiao-Lin Liu, Bo Liu, Chen Ni, J. Lumin. **132**, 2531–2536, (2012).

29. L.J. Borrero-González, L.A.O. Nunes, J.L. Carmo, F.B.G. Astrath, M.L. Baesso, J. Lumin. **145**, 615–619, (2014).

30. Hongli Wen, Peter A. Tanner, Opt. Mater. **33**, 1602–1606, (2011).

31. T. Guérineau, L. Loi, Y. Petit, S. Danto, A. Fargues, L. Canioni, T. Cardinal, Opt. Mater. Express **8**, 3748–3760, (2018).

32. N. Marquestaut, Y. Petit, A. Royon, P. Mounaix, T. Cardinal, L. Canioni, Adv. Func. Mater. **24**, 5824–5832, (2014).

33. V.K. Tikhomirov, T. Vosch, E. Fron, V.D. Rodríguez, J.J. Velázquez, D. Kirilenko, G. Van Tendeloo, J. Hofkens, M. Van der Auweraer, V.V. Moshchalkov, RSC Adv. **2**, 1496–1501, (2012).

34. J.J. Velázquez, V.K. Tikhomirov, L.F. Chibotaru, N.T. Cuong, A.S. Kuznetsov, V.D. Rodríguez, M.T. Nguyen, V.V. Moshchalkov, Opt. Express **12**, 13582–13591, (2012).